On Space–Frequency Correlation of UWB MIMO Channels

Xuemin Hong, Cheng-Xiang Wang, *Senior Member, IEEE*, John Thompson, *Member, IEEE*, Ben Allen, *Senior Member, IEEE*, Wasim Q. Malik, *Senior Member, IEEE*, and Xiaohu Ge, *Member, IEEE*

Abstract—Conventional multiple-input–multiple-output (MIMO) channel correlation models focus on describing the complex amplitude correlation of resolvable multipath components (MPCs). It has recently been shown that the time-of-arrival (ToA) correlation of resolvable MPCs, which has largely been ignored in the literature so far, is important for characterizing the space–frequency (SF) correlation of MIMO channels in the ultrawideband (UWB) regime. The proposal of ToA correlation brings forth the following open questions: What is the fundamental difference between amplitude and ToA correlations? Are they mutually replaceable? What impact do they have on system performance? Is this impact related to channel bandwidth? This paper systematically answers the above questions. We demonstrate that, compared with a conventional model that only considers amplitude correlation, a UWB MIMO channel model taking into account both amplitude and ToA correlations leads to different theoretical maximum diversity order, numerical structure of the SF channel covariance matrix, spatial correlation function, and diversity performance. We conclude that ToA correlation is a necessary complement to amplitude correlation when the channel bandwidth exceeds 500 MHz, i.e., UWB channels. This new insight serves as the motivation for more realistic modeling of UWB MIMO channels and the inspiration for designing advanced UWB MIMO systems to fully exploit the SF channel correlation properties.

Index Terms—Channel modeling, diversity order, multiple input–multiple output (MIMO), space–frequency (SF) correlation, ultrawideband (UWB).

I. Introduction

MULTIPLE input–multiple output (MIMO) is a promising wireless transmission technology that deploys multiple antennas at both ends of a communication link to increase the data rate or enhance the reliability without using additional power, bandwidth, or time slots [1]. For simplicity, MIMO channel models were often implemented by multiple uncorrelated Rayleigh fading processes [2], [3]. Unfortunately, the performance of MIMO systems is severely degraded by channel correlation, which is often encountered in practical situations due to insufficient antenna spacing or sparse scattering [1]. Consequently, an accurate and analytically tractable channel correlation model is required for the dependable design and performance analysis of realistic MIMO systems.

Different correlation models are required for narrow-band, wideband, and ultrawideband (UWB) MIMO channels [4]–[9]. In narrow-band systems, the physical multipath components (MPCs) are considered irresolvable, and the channel impulse response (CIR) is given by a complex-valued scalar channel coefficient, which represents the phase-shifted superposition of all MPCs. A narrow-band MIMO correlation model describes the correlation of the channel coefficients of MIMO subchannels. Examples of narrow-band MIMO correlation models include the Kronecker model [10], [11], joint correlation model [12], and virtual channel representation model [13]. The core element of a narrow-band MIMO correlation model is the spatial correlation function, which calculates the channel correlation coefficient as a function of antenna array parameters (e.g., antenna spacing, radiation pattern, etc.) and propagation environment (e.g., angular spread, scatterer distribution, etc.). A closed-form expression of the spatial correlation function is important for theoretical studies of MIMO system performance and has attracted considerable research interest [14]–[19].

Unlike narrow-band systems, wideband systems have finer delay resolution and a better capability to distinguish between the times-of-arrival (ToAs) of different MPCs. Therefore, a tapped-delay-line channel model is commonly used to describe a wideband CIR, where each tap represents a resolvable MPC characterized by a ToA and a complex amplitude. The ToA of a tap reflects a time bin in the delay domain, whereas the complex amplitude represents the phase-shifted superposition of multiple irresolvable MPCs in that time bin. Wideband MIMO correlation models [20], [21] assume that a resolvable

MPC (i.e., a tap) appears in different MIMO subchannels with varying (and possibly correlated) complex amplitudes but identical ToAs. The amplitude correlation of each tap can be specified using one of the aforementioned narrow-band MIMO correlation models.

Conventional UWB MIMO correlation models [22]–[25] adopt the same principle as the wideband MIMO correlation model and assume that the ToAs of a tap are identical in different MIMO subchannels. However, intuitively, this assumption becomes inappropriate in the UWB regime due to the very high delay resolution, which results in distinguishable ToA difference for a tap even between closely spaced antenna elements [26]. In our previous work [26], we proposed to take into account the effect of "ToA correlation" for UWB MIMO channel modeling. Simulation results showed that ToA correlation is essential in getting a space–frequency (SF) correlation pattern that better fits the measurements [27]–[30]. The introduction of ToA correlation into UWB MIMO channel modeling brings the following open questions: What is the fundamental difference between ToA correlation and the well-known complex amplitude correlation? Are they mutually replaceable? What impact do they have on the system performance? Is this impact related to the channel bandwidth? In [31], we partly answered the above questions from a theoretical perspective using a simplified UWB MIMO channel model, which neglected the effect of multipath clustering [32]. Multipath clustering refers to the propagation phenomenon that MPCs arriving from similar directions and delays are grouped into clusters. This is caused by the fact that scatterers tend to group together in realistic environments. In general, systems with larger bandwidths are expected to have stronger clustering effects due to a better time resolution [33]. In UWB channels, the clustering effect is typically quite significant [34]–[36].

Extending our previous work [31], this paper investigates the SF correlation of UWB MIMO channels using a more realistic channel model that considers multipath clustering. Moreover, we systematically discuss the differences and relations of ToA and amplitude correlations based on physical intuition, theoretical analysis, numerical demonstrations, and simulation results. The following contributions are made in this paper. First, we propose a new UWB MIMO correlation model that provides better accuracy than the model in [31], while maintaining the analytical tractability. Second, we explain from various perspectives the difference between ToA correlation and complex amplitude correlation, and clarify their impact on the SF correlation of UWB MIMO channels. Third, we theoretically prove that, different from wideband MIMO systems [21] and previous understandings for UWB MIMO systems [22], the maximum diversity order of SF coded UWB MIMO systems over clustered multipath channels is not affected by the degree of multipath amplitude correlation.

The remainder of this paper is organized as follows. In Section II, we first provide an intuitive explanation for the causes of ToA and amplitude correlations in MIMO channels. Section III introduces the proposed UWB MIMO channel correlation model. Section IV analyzes the structure of the resulting SF channel covariance matrix. In Section V, we apply the proposed correlation model to study the maximum diversity
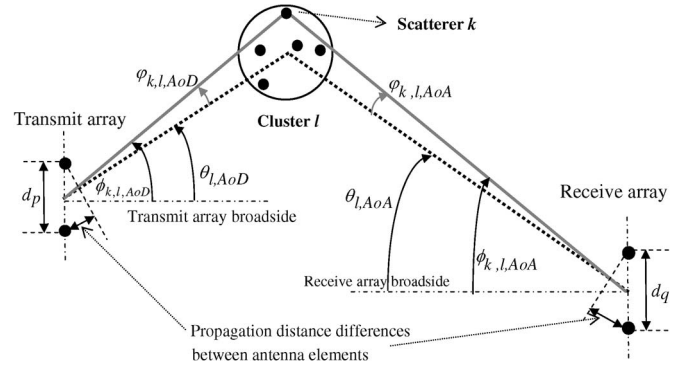

Fig. 1. Angular parameters in clustered multipath channels and the physical propagation phenomenon causing the multipath ToA variation/correlation.

order of SF coded UWB MIMO systems. Numerical and simulation results are provided in Section VI, and conclusions are drawn in Section VII.

II. TIME OF ARRIVAL CORRELATION AND AMPLITUDE CORRELATION

Unlike amplitude correlation, ToA correlation is a less-discussed concept in the literature. Therefore, here, we first provide an intuitive explanation of ToA correlation and discuss its relationship with amplitude correlation and system bandwidth. Fig. 1 illustrates the propagation path of a typical (single-bounce) physical MPC in a MIMO system. Due to the differences of the propagation path length, an impinging MPC may have different ToAs in different MIMO subchannels. These ToAs are "correlated" in the sense that their mutual differences are determined by the small propagation delays across antenna elements. Such propagation delays depend on the geometries of the transmit/receive antenna arrays, as well as the directional property of the MPC. A 30-cm antenna spacing, for example, can cause a maximum propagation delay of 1 ns, which is larger than the temporal resolution of a UWB system.

In an ideal system with infinite bandwidth, every physical MPC is resolvable and can be described by a Dirac delta function with a real-valued amplitude and a ToA. An MPC appears in different MIMO subchannels with identical amplitudes but different ToAs. Illustrating four MPCs, Fig. 2 shows an example of the ideal CIRs of two correlated MIMO subchannels. The xth ($x = 1, 2, 3, 4$) MPC is denoted as δ_x in the first MIMO subchannel and as $\tilde{\delta}_x$ in the second MIMO subchannel. A proper metric to describe the "correlation" of the two CIRs is their MPC ToA differences.

Now, let us consider a wideband MIMO system whose CIR is given by a tapped-delay-line structure, where each tap represents a resolvable MPC that is characterized by a ToA and a complex-valued amplitude. The ToA of a tap reflects a time bin in the delay domain, whereas the complex amplitude of a tap represents the phase-shifted superposition of multiple irresolvable MPCs in that time bin. The width of the time bin is inversely proportional to the bandwidth of the system. Fig. 2 illustrates how the ideal CIRs are converted into wideband CIRs with two taps (i.e., resolvable MPCs). The first tap captures δ_1 and δ_2 in the first MIMO subchannel, as well as their
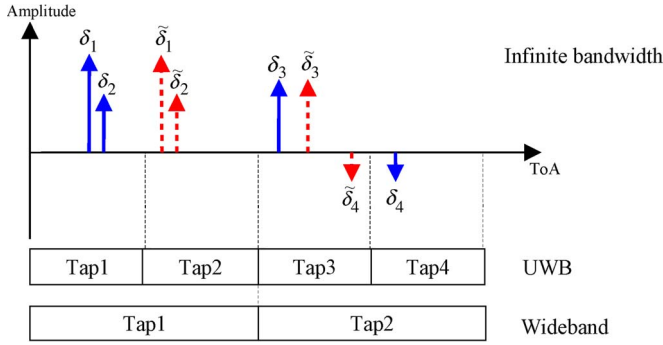
Fig. 2. ToA correlation and amplitude correlation in two MIMO subchannels with different system bandwidths.

time-shifted copies $\tilde{\tilde{\delta}}_1$ and $\tilde{\tilde{\delta}}_2$ in the second MIMO subchannel. We can, therefore, consider this tap as having identical ToAs in the two MIMO subchannels but varying complex amplitudes caused by the phase changes of superposing irresolvable MPCs. In a typical wideband system, the width of the time bin is relatively wide so that most of the multipath ToA differences are indistinguishable. In this case, the correlation between two MIMO subchannels can be fully characterized by the complex amplitude correlation.

When the system bandwidth increases to the UWB regime, the ToA difference of an MPC may eventually become distinguishable due to better delay resolution. This is illustrated in Fig. 2 with a four-tap UWB channel. Unlike the two-tap wideband channel, δ_1 and δ_2 and their copies $\tilde{\tilde{\delta}}_1$ and $\tilde{\tilde{\delta}}_2$ now fall into different time bins. This necessitates the introduction of ToA correlation. Meanwhile, unlike the ideal CIR, a tap within a UWB channel may still consist of a number of irresolvable MPCs (e.g., δ_1 and δ_2 in the first tap) so that the use of complex amplitude correlation is also justified. In fact, Fig. 2 suggests that the amplitude correlation and the ToA correlation can play different roles to capture the "irresolvable" and "resolvable" correlation effects of the underlying MPCs, respectively. Inspired by this intuition, in what follows, we will present a generalized correlation model that incorporates both the multipath amplitude and ToA correlations.

III. GENERALIZED ULTRAWIDEBAND MULTIPLE-INPUT–MULTIPLE-OUTPUT CHANNEL CORRELATION MODEL

We consider a clustered $M_t \times M_r$ wideband/UWB MIMO channel with M_t and M_r transmit and receive antenna elements, respectively. The CIR from the pth $(p = 1, 2, \ldots, M_t)$ transmit antenna to the qth $(q = 1, 2, \ldots, M_r)$ receive antenna is given by

$$h^{p,q}(t) = \sum_{l=0}^{L-1} \sum_{k=0}^{K-1} a_{l,k}^{p,q} \delta(t - \tau_{l,k} - \epsilon_{l,k}^{p,q}) \qquad (1)$$

where L is the number of clusters, l $(l = 0, 1, 2, \ldots, L-1)$ is the cluster index, K is the number of resolvable MPCs (or "taps") in a cluster, k $(k = 0, 1, 2, \ldots, K-1)$ is the MPC index within a cluster, $a_{l,k}^{p,q}$ is the amplitude coefficient of the kth MPC of the lth cluster, $\tau_{l,k}$ is the reference ToA of the corresponding MPC (i.e., the ToA with respect to the array

center), and $\epsilon_{l,k}^{p,q}$ is the ToA difference with respect to $\tau_{l,k}$. As discussed in Section II, in conventional tapped-delay-line wideband MIMO channel models, $a_{l,k}^{p,q}$ have varying (possibly correlated) complex values in different MIMO subchannels, whereas $\epsilon_{l,k}^{p,q} = 0$. In ideal CIRs for systems with infinite bandwidth, $a_{l,k}^{p,q}$ have identical real values in different MIMO subchannels, whereas $\epsilon_{l,k}^{p,q} \neq 0$. In this paper, we consider a band-limited MIMO system to give (possibly correlated) complex-valued $a_{l,k}^{p,q}$ and nonzero valued $\epsilon_{l,k}^{p,q}$. Our formulation is more general and can be applied to wideband as well as UWB channels.

The amplitude correlation of the kth MPC of the lth cluster is characterized by an $M_t M_r \times M_t M_r$ covariance matrix $\mathbf{R}_{l,k}^A$ given by

$$\mathbf{R}_{l,k}^A = \mathbb{E}\left\{ \mathbf{a}_{l,k} \mathbf{a}_{l,k}^\dagger \right\} \qquad (2)$$

where $\mathbb{E}\{\cdot\}$ denotes expectation, and $[\cdot]^\dagger$ stands for the Hermitian transpose of a matrix/vector. In (2), $\mathbf{a}_{l,k}$ is an $M_t M_r \times 1$ vector that is formatted as

$$\mathbf{a}_{l,k} = \left[a_{l,k}^{1,1}, \ldots, a_{l,k}^{1,M_r}, a_{l,k}^{2,1}, \ldots, a_{l,k}^{M_t,1}, \ldots, a_{l,k}^{M_t,M_r} \right]^T \qquad (3)$$

where $[\cdot]^T$ stands for the matrix transpose. An entry of $\mathbf{R}_{l,k}^A$ is given by

$$
\begin{aligned}
\left[\mathbf{R}_{l,k}^A \right]_{p_1 q_1, p_2 q_2} &= \chi_{l,k}^{p_1 q_1, p_2 q_2} \\
&= \mathbb{E}\left\{ a_{l,k}^{p_1, q_1} \left(a_{l,k}^{p_2, q_2} \right)^* \right\} \\
&= \xi_{l,k}^{p_1 q_1, p_2 q_2} \sigma_{l,k}^2 \qquad (4)
\end{aligned}
$$

where $p_1, p_2 = 1, 2, \ldots, M_t$, $q_1, q_2 = 1, 2, \ldots, M_r$, $(\cdot)^*$ denotes the complex conjugate, $\xi_{l,k}^{p_1 q_1, p_2 q_2}$ is the correlation coefficient between random variables $a_{l,k}^{p_1, q_1}$ and $a_{l,k}^{p_2, q_2}$, and $\sigma_{l,k}^2 = \mathbb{E}\{|a_{l,k}^{p_1, q_1}|^2\} = \mathbb{E}\{|a_{l,k}^{p_2, q_2}|^2\}$ is the variance/power of the kth MPC in the lth cluster.

ToA correlation can be introduced by assigning proper values to the ToA difference $\epsilon_{l,k}^{p,q}$ in (1). As illustrated in Fig. 1, we assume that, for each MPC, its ToA variation in different MIMO subchannels is only caused by the difference of propagation delays across the antenna elements at the transmit and receive arrays. Therefore, given the geometries of transmit/receive arrays and the multipath angle of arrival (AoA) and angle of departure (AoD), the corresponding ToA variation can be fully specified. For simplicity, in this paper, we restrict our discussion to uniform linear arrays (ULAs), noting that generalizations to other types of arrays are straightforward. It follows that $\epsilon_{l,k}^{p,q}$ can be evaluated as [26]

$$\epsilon_{l,k}^{p,q} = [d_p \sin(\phi_{l,k,\mathrm{AoD}}) + d_q \sin(\phi_{l,k,\mathrm{AoA}})]/c \qquad (5)$$

where c is the speed of light, d_p and d_q are the transmit and receive antenna spacings, respectively, and $\phi_{l,k,\mathrm{AoA}}$ and $\phi_{l,k,\mathrm{AoD}}$ are the AoA and the AoD of the kth MPC of the lth cluster, respectively. Similar to the hierarchical angular model that is used in the Third Generation Partnership Project (3GPP) spatial channel model [37], we have

$$\phi_{k,l,\mathrm{AoA}} = \theta_{l,\mathrm{AoA}} + \varphi_{k,l,\mathrm{AoA}} \qquad (6)$$

$$\phi_{k,l,\mathrm{AoD}} = \theta_{l,\mathrm{AoD}} + \varphi_{k,l,\mathrm{AoD}} \qquad (7)$$

where $\theta_{l,\text{AoA}}$ and $\theta_{l,\text{AoD}}$ are the mean AoA and AoD of the lth cluster, and $\varphi_{k,l,\text{AoA}}$ and $\varphi_{k,l,\text{AoD}}$ are the offset angles for the kth MPC of the lth cluster with respect to $\theta_{l,\text{AoA}}$ and $\theta_{l,\text{AoD}}$, respectively. The relationship of these angle parameters is illustrated in Fig. 1. Due to random antenna orientations and cluster locations, $\theta_{l,\text{AoA}}$ and $\theta_{l,\text{AoD}}$ typically follow uniform distributions from 0 to 2π, which is supported by a number of directional UWB channel measurements [35], [36]. Meanwhile, various distributions such as uniform, truncated Gaussian, truncated Laplacian, and von-Mises distributions [18], [19] have been proposed to describe $\varphi_{k,l,\text{AoA}}$ or $\varphi_{k,l,\text{AoD}}$. For example, a Laplacian distribution with a zero-mean and an angle spread (AS) of $38°$ is observed in [35] for UWB channels in an office/laboratory environment.

From (6) and (7), we can see that $\phi_{k,l,\text{AoD}}$ and $\phi_{k,l,\text{AoA}}$ have two levels of randomness due to their hierarchical composition. In some cases, we are interested in a static scenario where the locations of main clusters are fixed, i.e., $\theta_{l,\text{AoA}}$ and $\theta_{l,\text{AoD}}$ are treated as deterministic. Therefore, the mean values of $\phi_{k,l,\text{AoA}}$ and $\phi_{k,l,\text{AoD}}$ are given by $\theta_{l,\text{AoA}}$ and $\theta_{l,\text{AoD}}$, whereas the shapes of their probability density function (pdf) are determined by $\varphi_{k,l,\text{AoA}}$ and $\varphi_{k,l,\text{AoD}}$, respectively. In other cases, we may be interested in a dynamic scenario with moving transmitters/receivers or scatters. It is then desirable to treat $\theta_{l,\text{AoA}}$ and $\theta_{l,\text{AoD}}$ as random variables. When $\theta_{l,\text{AoA}}$ and $\theta_{l,\text{AoD}}$ are uniformly distributed from 0 to 2π, it follows that $\phi_{k,l,\text{AoD}}$ and $\phi_{k,l,\text{AoA}}$ also have uniform distributions from 0 to 2π.

In channel modeling, there is a tradeoff on the model accuracy and analytical tractability. In this paper, we would like to have an analytically tractable channel correlation model with improved accuracy compared with the model in [31]. To this end, the following assumptions are made.

1) The fading amplitudes of different MPCs are independent, i.e., $\mathbb{E}\{a_{l_1,k_1}^{p_1,q_1}(a_{l_2,k_2}^{p_2,q_2})^*\} = 0$, given that $l_1 \neq l_2$ or $k_1 \neq k_2$. This is a common assumption following the widely applied uncorrelated scatterer model. Although the fading of different MPCs is more likely to be correlated when the system bandwidth increases, experiments [38] did not find significant correlation even in UWB channels.

2) The fading amplitude, ToA, and angular statistics of an MPC are mutually independent. This is a widely used assumption in the literature (e.g., [20]–[22]) to simplify the channel model.

3) Given the mean AoA/AoD of a cluster, the AoAs/AoDs of different MPCs within the cluster are independent and identically distributed. This is a natural conclusion following the hierarchical angular model described by (6) and (7).

4) A Kronecker correlation model [10] is used to describe the complex amplitude correlation of a tap. This can be justified from two aspects. First, the Kronecker model assumes that the transmitter and receiver side correlations are independent. Using measured results of the bit-error-rate (BER) performance, the applicability of the Kronecker model to UWB channels has been indirectly verified in [25]. Second, in this paper, the Kronecker

model is used to describe the correlation of a single tap, which comes from a single cluster with a small AS. In this case, the Kronecker model can give a good approximation to the actual channel correlation [40]. We also note that the Kronecker model can be used to characterize the correlation of not only Gaussian fading taps but other fading types as well, such as lognormal and Nakagami fading.

IV. STRUCTURE OF THE SPACE–FREQUENCY CHANNEL COVARIANCE MATRIX

Given the CIR in (1), the corresponding channel frequency response $H^{p,q}(f)$ can be obtained via the Fourier transform. Considering UWB MIMO systems that employ orthogonal frequency-division multiplexing (OFDM) [22], we are interested in the discretized channel frequency response $H^{p,q}(n)$ given by

$$H^{p,q}(n) = \sum_{l=0}^{L-1} \sum_{k=0}^{K-1} a_{l,k}^{p,q} \exp\left[-j2\pi n \Delta f \left(\tau_{l,k} + \epsilon_{l,k}^{p,q}\right)\right] \quad (8)$$

where Δf denotes the subcarrier frequency spacing, $n = 1, 2, \ldots, N$ denotes the subcarrier index, and N denotes the total number of subcarriers. The channel vector $\mathbf{H}$ of size $M_t M_r N \times 1$ is given by

$$\mathbf{H} = \left[\mathbf{H}^{1,1}, \ldots, \mathbf{H}^{1,M_r}, \ldots, \mathbf{H}^{p,q}, \ldots, \mathbf{H}^{M_t,M_r}\right]^T \quad (9)$$

where $\mathbf{H}^{p,q}$ is an $N \times 1$ vector given by

$$\mathbf{H}^{p,q} = \left[H^{p,q}(1), H^{p,q}(2), \ldots, H^{p,q}(N)\right]. \quad (10)$$

We then have $\mathbf{R} = \mathbb{E}\{\mathbf{H}\mathbf{H}^{\dagger}\}$ as the channel covariance matrix, which is of size $M_t M_r N \times M_t M_r N$ and is referred to as the SF channel covariance matrix in this paper.

A. Entries of $\mathbf{R}$

Consider an arbitrary entry of $\mathbf{R}$ given by

$$[\mathbf{R}]_{p_1 q_1 n_1, p_2 q_2 n_2} = \rho^{p_1 q_1 n_1, p_2 q_2 n_2}$$
$$= \mathbb{E}\left\{H^{p_1,q_1}(n_1)\left[H^{p_2,q_2}(n_2)\right]^*\right\} \quad (11)$$

where $n_1, n_2 = 1, 2, \ldots, N$. Substituting (8) into (11), it follows that

$$\rho^{p_1 q_1 n_1, p_2 q_2 n_2} = \sum_{l=0}^{L-1} \alpha_l^{p_1 q_1 n_1, p_2 q_2 n_2} \beta_l^{p_1 q_1 n_1, p_2 q_2 n_2} \quad (12)$$

where

$$\alpha_l^{p_1 q_1 n_1, p_2 q_2 n_2} = \sum_{k=0}^{K-1} \chi_{l,k}^{p_1 q_1, p_2 q_2} \exp\left[-j2\pi \Delta f(n_1 - n_2)\tau_{l,k}\right] \quad (13)$$

is a coefficient that is related to the amplitude correlation, and

$$\beta_l^{p_1 q_1 n_1, p_2 q_2 n_2} = \mathbb{E}\left\{\exp\left[-j2\pi \Delta f\left(n_1 \epsilon_{l,k}^{p_1,q_1} - n_2 \epsilon_{l,k}^{p_2,q_2}\right)\right]\right\} \quad (14)$$

is a coefficient that is related to the ToA correlation. If the ToA correlation/differences are not taken into account, i.e., $\epsilon_{l,k}^{p_1,q_1} = \epsilon_{l,k}^{p_2,q_2} = 0$, it follows that $\beta_l^{p_1q_1n_1,p_2q_2n_2} = 1$, and (12) is reduced to $\rho^{p_1q_1n_1,p_2q_2n_2} = \sum_{l=0}^{L-1} \alpha_l^{p_1q_1n_1,p_2q_2n_2}$, which represents the case using conventional MIMO correlation models.

Substituting (5) into (14) and using the assumption of AoA–AoD independence, we get

$$\beta_l^{p_1q_1n_1,p_2q_2n_2} = \beta_l^{p_1n_1,p_2n_2} \beta_l^{q_1n_1,q_2n_2}. \tag{15}$$

In (15), we have

$$\beta_l^{p_1n_1,p_2n_2} = \mathbb{E}\{\exp[-jx_p\sin(\phi_{l,k,\text{AoD}})]\} \tag{16}$$

$$\beta_l^{q_1n_1,q_2n_2} = \mathbb{E}\{\exp[-jx_q\sin(\phi_{l,k,\text{AoA}})]\} \tag{17}$$

where the expectations are taken over $\phi_{l,k,\text{AoD}}$ and $\phi_{l,k,\text{AoA}}$, respectively, and

$$x_p = 2\pi\Delta f(n_1 d_{p_1} - n_2 d_{p_2})/c \tag{18}$$

$$x_q = 2\pi\Delta f(n_1 d_{q_1} - n_2 d_{q_2})/c \tag{19}$$

denote the normalized SF distances at the transmitter and the receiver, respectively. Corresponding to the two levels of randomness described by (6) and (7), we will address two cases of AoA/AoD distributions. The first case is also the simplest case, where $\phi_{l,k,\text{AoD}}$ and $\phi_{l,k,\text{AoA}}$ are both assumed to have uniform distributions from 0 to 2π. As previously discussed in Section II, this may represent a dynamic environment with isotropic scattering. It follows that

$$\beta_l^{p_1n_1,p_2n_2} = J_0(x_p) \tag{20}$$

$$\beta_l^{q_1n_1,q_2n_2} = J_0(x_q) \tag{21}$$

where $J_0(\cdot)$ is the zeroth-order Bessel function of the first kind. The second case that we considered represents a static scenario where the mean AoA and AoD of a cluster are fixed, whereas the AoAs and AoDs within a cluster follow Laplacian distributions. It follows that the pdf's of $\phi_{l,k,\text{AoD}}$ and $\phi_{l,k,\text{AoA}}$ of the lth cluster are given by

$$P(\phi_{l,k,\text{AoA}}) = \frac{1}{\sqrt{2}\kappa_{l,\text{AoA}}}$$

$$\times \exp\left\{-\frac{\sqrt{2}|\phi_{l,k,\text{AoA}} - \theta_{l,k,\text{AoA}}|}{\kappa_{l,\text{AoA}}}\right\} \tag{22}$$

$$P(\phi_{l,k,\text{AoD}}) = \frac{1}{\sqrt{2}\kappa_{l,\text{AoD}}}$$

$$\times \exp\left\{-\frac{\sqrt{2}|\phi_{l,k,\text{AoD}} - \theta_{l,k,\text{AoD}}|}{\kappa_{l,\text{AoD}}}\right\} \tag{23}$$

respectively, where $|\cdot|$ denotes the absolute-value operation, $\kappa_{l,\text{AoA}}$ and $\kappa_{l,\text{AoD}}$ are the ASs of the lth cluster, respectively, and $\theta_{l,k,\text{AoA}}$ and $\theta_{l,k,\text{AoD}}$ are the mean AoA and AoD of the lth cluster, respectively. From (16), (17), (22), and (23) and following similar steps in [17], we have

$$\beta_l^{p_1n_1,p_2n_2} = J_{\text{Re}}(x_p) + iJ_{\text{Im}}(x_p) \tag{24}$$

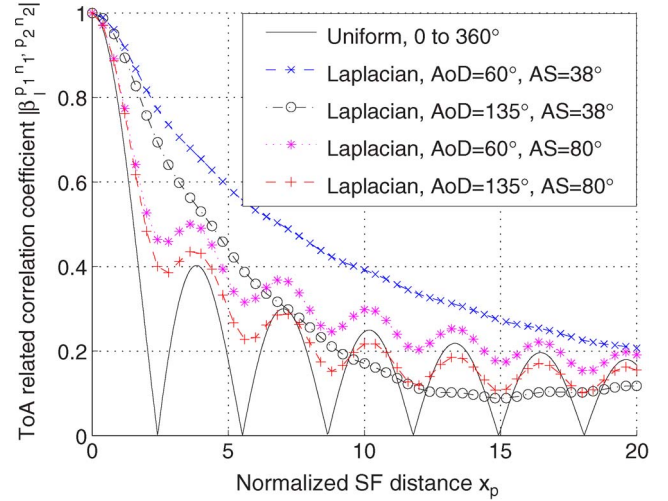$$\beta_l^{q_1n_1,q_2n_2} = J_{\text{Re}}(x_q) + iJ_{\text{Im}}(x_q) \tag{25}$$

Fig. 3. Absolute values of the ToA-related coefficients $|\beta_l^{p_1n_1,p_2n_2}|$ [given by (20) and (24)] as functions of the normalized SF distance x_p, with different sets of angular parameters.

where $i = \sqrt{-1}$, and $J_{\text{Re}}(\cdot)$ and $J_{\text{Im}}(\cdot)$ are functions that are defined as

$$J_{\text{Re}}(x) = J_0(x) + 2\sum_{m=1}^{\infty} \frac{J_{2m}(x)}{1 + 2m^2\kappa_{l,\text{AoA}}^2}\cos(2m\theta_{l,\text{AoA}}) \tag{26}$$

$$J_{\text{Im}}(x) = 4\sum_{m=0}^{\infty} \frac{J_{2m+1}(x)}{2 + (2m+1)^2\kappa_{l,\text{AoA}}^2}\sin[(2m+1)\theta_{l,\text{AoA}}] \tag{27}$$

where $J_z(\cdot)$ is the zth-order Bessel function of the first kind. When computing the infinite summations in (26) and (27), we can use $m = 100$ to obtain sufficient accuracy [39]. In Fig. 3, $|\beta_l^{p_1n_1,p_2n_2}|$ is computed from (20) and (24) as a function of x_p with different sets of angular parameters. It is observed that with a decreasing AS, $|\beta_l^{q_1n_1,q_2n_2}(x_p)|$ tends to have bigger values and smoother curves.

B. Decomposition of **R**

Here, we will show that the channel covariance matrix **R** can be decomposed into more tractable smaller matrices. This property gives the proposed channel model the advantage to facilitate theoretical analysis of UWB MIMO systems. From (12), we can write

$$\mathbf{R} = \sum_{l=0}^{L-1} \mathbf{R}_l = \sum_{l=0}^{L-1} \mathbf{A}_l \circ \mathbf{B}_l \tag{28}$$

where $\mathbf{R}_l = \mathbf{A}_l \circ \mathbf{B}_l$ is the SF covariance matrix with respect to the lth cluster, $\circ$ denotes the Hadamard product, $\mathbf{A}_l$ is an $M_t M_r N \times M_t M_r N$ matrix whose entries are given by $\alpha_l^{p_1q_1n_1,p_2q_2n_2}$, and $\mathbf{B}_l$ is also an $M_t M_r N \times M_t M_r N$ matrix whose entries are given by $\beta_l^{p_1q_1n_1,p_2q_2n_2}$. From (13), it can be shown that $\mathbf{A}_l$ can be written as

$$\mathbf{A}_l = (\mathbf{I}_{M_tM_r} \otimes \mathbf{W}_l)\mathbf{\Phi}_l(\mathbf{I}_{M_tM_r} \otimes \mathbf{W}_l^H) \tag{29}$$

where $\otimes$ denotes the Kronecker product, and $\mathbf{I}_{M_t M_r}$ is the $M_t M_r \times M_t M_r$ identity matrix. Matrix $\mathbf{W}_l$ is an $N \times K$ Fourier matrix, which is defined as

$$\mathbf{W}_l = \begin{bmatrix} 1 & 1 & \cdots & 1 \\ w^{\tau_{l,0}} & w^{\tau_{l,1}} & \cdots & w^{\tau_{l,K-1}} \\ \vdots & \vdots & \ddots & \vdots \\ w^{(N-1)\tau_{l,0}} & w^{(N-1)\tau_{l,1}} & \cdots & w^{(N-1)\tau_{l,K-1}} \end{bmatrix} \tag{30}$$

where $w = \exp(-j2\pi\Delta f)$. Matrix $\boldsymbol{\Phi}_l$ is an $M_t M_r K \times M_t M_r K$ square matrix, which is defined as

$$\boldsymbol{\Phi}_l = \begin{bmatrix} \mathbf{V}_l^{1111} & \mathbf{V}_l^{1112} & \cdots & \mathbf{V}_l^{11M_t M_r} \\ \mathbf{V}_l^{1211} & \mathbf{V}_l^{1212} & \cdots & \mathbf{V}_l^{12M_t M_r} \\ \vdots & \vdots & \mathbf{V}_l^{p_1 q_1 p_2 q_2} & \vdots \\ \mathbf{V}_l^{M_t M_r 11} & \mathbf{V}_l^{M_t M_r 12} & \cdots & \mathbf{V}_l^{M_t M_r M_t M_r} \end{bmatrix} \tag{31}$$

where $\mathbf{V}_l^{p_1 q_1 p_2 q_2}$ is a $K \times K$ diagonal matrix, which is given by

$$\mathbf{V}_l^{p_1 q_1 p_2 q_2} = \mathrm{diag}\left\{\chi_{l,0}^{p_1 q_1, p_2 q_2}, \chi_{l,1}^{p_1 q_1, p_2 q_2}, \ldots, \chi_{l,K-1}^{p_1 q_1, p_2 q_2}\right\}. \tag{32}$$

In (32), $\chi_{l,k}^{p_1 q_1, p_2 q_2}$ is the multipath amplitude covariance coefficient defined in (4).

Now, let us consider the structure of matrix $\mathbf{B}_l$. In the case that AoAs and AoDs are uniformly distributed from 0 to 2π, matrix $\mathbf{B}_l$ can be written from (20) and (21) as

$$\mathbf{B}_l = J_0(\mathbf{X}_p) \circ J_0(\mathbf{X}_q). \tag{33}$$

Here, $\mathbf{X}_p$ and $\mathbf{X}_q$ are $M_t M_r N \times M_t M_r N$ normalized SF distance matrices, which are given by

$$\mathbf{X}_p = \frac{2\pi\Delta f}{c}(\mathbf{P} - \mathbf{P}^T) \tag{34}$$

$$\mathbf{X}_q = \frac{2\pi\Delta f}{c}(\mathbf{Q} - \mathbf{Q}^T) \tag{35}$$

respectively, where $\mathbf{P}$ and $\mathbf{Q}$ are both $M_t M_r N \times M_t M_r N$ matrices defined as

$$\mathbf{P} = \mathbf{d}_T \otimes \mathbf{1}_{M_t M_r N \times M_r} \otimes \mathbf{d}_N \tag{36}$$

$$\mathbf{Q} = \mathbf{1}_{M_t M_r N \times M_r} \otimes \mathbf{d}_R \otimes \mathbf{d}_N \tag{37}$$

respectively. It is noted that the operator $J_0(\cdot)$ in (33) computes the zeroth-order Bessel function of the first kind for each element of the input matrix. In (36) and (37), $\mathbf{d}_N = [1, 2, \ldots, N]$ is the $1 \times N$ subcarrier index vector, and $\mathbf{1}_{M_t M_r N \times M_r}$ is an $M_t M_r N \times M_r$ matrix with unit entries. Vectors $\mathbf{d}_T = d_p([0, 1, \ldots, M_t - 1] - (M_t - 1)/2)$ and $\mathbf{d}_R = d_q([0, 1, \ldots, M_r - 1] - (M_r - 1)/2)$ denote the $1 \times M_t$ transmit antenna spacing vector and $1 \times M_r$ receive antenna spacing vector, respectively, with respect to the array center. Here, d_p and d_q denote the spacings between adjacent antenna elements in the transmit and receive ULAs, respec-

tively. Similarly, in the case of Laplacian-distributed AoAs and AoDs, from (24) and (25), we have

$$\mathbf{B}_l = [J_{\mathrm{Re}}(\mathbf{X}_p) + iJ_{\mathrm{Im}}(\mathbf{X}_p)] \circ [J_{\mathrm{Re}}(\mathbf{X}_q) + iJ_{\mathrm{Im}}(\mathbf{X}_q)]. \tag{38}$$

V. MAXIMUM DIVERSITY ORDER OF ULTRAWIDEBAND MULTIPLE-INPUT–MULTIPLE-OUTPUT SYSTEMS

Due to the tractable structure of the SF channel covariance matrix, we are able to investigate the maximum achievable diversity order in UWB MIMO channels. We consider SF coding across M_t transmit antennas and N OFDM subcarriers. Each codeword $\mathbf{C}$ is then an $N \times M_t$ matrix given by [20]

$$\mathbf{C} = \begin{bmatrix} c^1(1) & c^2(1) & \cdots & c^{M_t}(1) \\ c^1(2) & c^2(2) & \cdots & c^{M_t}(2) \\ \vdots & \vdots & c^p(k) & \vdots \\ c^1(N) & c^2(N) & \cdots & c^{M_t}(N) \end{bmatrix} \tag{39}$$

where $c^p(n)$ represents the symbol that is transmitted over the nth subcarrier by the pth transmit antenna. At the receiver, after matched filtering, removing the cyclic prefix, and applying the discrete Fourier transform, the received signal at the nth subcarrier and the qth receive antenna is given by

$$y^q(n) = \sqrt{\frac{\rho}{M_t}} \sum_{p=1}^{M_t} c^p(n) H^{p,q}(n) + z^q(n) \tag{40}$$

where ρ is the average signal-to-noise ratio, and $z^q(n)$ denotes the additive white complex Gaussian noise with zero mean and unit variance at the nth subcarrier and the qth receive antenna. We can further write the receive signal as [20]

$$\mathbf{Y} = \sqrt{\frac{\rho}{M_t}} \mathbf{D} \mathbf{H} + \mathbf{Z} \tag{41}$$

where the received vector $\mathbf{Y}$ of size $NM_r \times 1$ is given by

$$\mathbf{Y} = \left[y^1(0), \ldots, y^1(N-1), \ldots, y^q(k), \ldots, y^{M_r}(N-1)\right]^T. \tag{42}$$

In (41), $\mathbf{H}$ is the channel frequency response vector formatted in (9), $\mathbf{Z}$ is the corresponding noise vector, and $\mathbf{D}$ is an $NM_r \times NM_t M_r$ matrix constructed from the SF codeword $\mathbf{C}$ as follows:

$$\mathbf{D} = \mathbf{I}_{M_t} \otimes [\mathbf{D}^1, \mathbf{D}^2, \ldots, \mathbf{D}^q, \ldots, \mathbf{D}^{M_r}]. \tag{43}$$

Here, $\mathbf{I}_{M_t}$ is an identity matrix of size $M_t \times M_t$, and $\mathbf{D}^q = \mathrm{diag}\{c^q(0), c^q(1), \ldots, c^q(N-1)\}$ for any $q = 1, 2, \ldots, M_r$.

The maximum achievable diversity or full diversity is defined as the maximum diversity order that can be achieved by SF codes of size $N \times M_t$. In this paper, we only discuss the maximum diversity order as an upper bound of the maximum achievable diversity without discussing whether the upper bound is achievable. Suppose that $\mathbf{D}$ and $\tilde{\mathbf{D}}$ are two matrices that are constructed from two different codewords $\mathbf{C}$

and $\tilde{\mathbf{C}}$, respectively. The maximum diversity order Λ can then be determined as [20]

$$\Lambda = \text{rank}\left\{ (\mathbf{D} - \tilde{\mathbf{D}})\mathbf{R}(\mathbf{D} - \tilde{\mathbf{D}})^\dagger \right\}. \qquad (44)$$

According to the rank inequalities on matrix multiplication [42], we have

$$\Lambda \leq \min\left\{ M_r N, \text{rank}(\mathbf{R}) \right\}. \qquad (45)$$

From (28) and based on the rank inequalities on matrix addition and Hadamard product [42], we get

$$\text{rank}(\mathbf{R}) \leq \sum_{l=0}^{L-1} \text{rank}(\mathbf{R}_l) \leq \sum_{l=0}^{L-1} \text{rank}(\mathbf{A}_l)\text{rank}(\mathbf{B}_l). \qquad (46)$$

Since $\mathbf{A}_l$ can be further decomposed as shown in (29), based on rank inequalities on matrix Kronecker product [42], it follows that

$$\text{rank}(\mathbf{A}_l) \leq \min\left\{ \text{rank}(\mathbf{I}_{M_r} \otimes \mathbf{W}_l), \text{rank}(\mathbf{\Phi}_l) \right\}$$
$$\leq \min\left\{ M_t M_r \min\{N, K\}, \text{rank}(\mathbf{\Phi}_l) \right\}. \qquad (47)$$

In (47), $\mathbf{\Phi}_l$ is the $M_t M_r K \times M_t M_r K$ matrix given by (31). Applying matrix permutations to $\mathbf{\Phi}_l$ can yield another matrix, i.e.,

$$\tilde{\mathbf{\Phi}}_l = \mathbf{I}_K \otimes \left[\mathbf{R}_{l,0}^A, \mathbf{R}_{l,1}^A, \ldots, \mathbf{R}_{l,K-1}^A \right] \qquad (48)$$

where $\mathbf{R}_{l,k}^A$ defined in (2) is the amplitude covariance matrix of the kth MPC of the lth cluster. From (48), it follows that

$$\text{rank}(\mathbf{\Phi}_l) = \text{rank}(\tilde{\mathbf{\Phi}}_l) \leq \sum_{k=0}^{K-1} \text{rank}\left(\mathbf{R}_{l,k}^A \right). \qquad (49)$$

Substituting (46), (47), and (49) into (45), we get

$$\Lambda \leq \min\left\{ M_r N, \sum_{l=0}^{L-1} \text{rank}(\mathbf{B}_l) \sum_{k=0}^{K-1} \text{rank}\left(\mathbf{R}_{l,k}^A \right) \right\}. \qquad (50)$$

In the case of conventional wideband MIMO channel models (no ToA correlation), we have $\text{rank}(\mathbf{B}_l) = 1$, and

$$\Lambda \leq \min\left\{ M_r N, \sum_{l=0}^{L-1} \sum_{k=0}^{K-1} \text{rank}\left(\mathbf{R}_{l,k}^A \right) \right\} \qquad (51)$$

which is in agreement with the result in [21]. In (51), $M_r N$ is as a constraint imposed by the system design, whereas $\sum_{l=0}^{L-1} \sum_{k=0}^{K-1} \text{rank}(\mathbf{R}_{l,k}^A)$ is a constraint imposed by the propagation channel. Given a fixed number of antenna elements and a sufficiently large OFDM size $N > M_t LK$, (51) reveals that the diversity order of a MIMO system depends on the number of taps (i.e., LK), as well as the degree of their amplitude correlation.

To analyze the maximum diversity order of MIMO channels with ToA correlation, we need to determine the rank of $\mathbf{B}_l$ in (50). Let us consider a simple case with $N = 1$, bearing in mind that larger values of N can only increase the rank. In the case of a uniform AoA/AoD distribution, substituting (36) and (37) into

(33) and taking $N = 1$, after some mathematical manipulations, we get

$$\mathbf{B}_l = J_0\left(\frac{2\pi d_t \Delta f}{c} \mathbf{U}_{M_t} \right) \otimes J_0\left(\frac{2\pi d_q \Delta f}{c} \mathbf{U}_{M_r} \right) \qquad (52)$$

where $\mathbf{U}_{M_t}$ and $\mathbf{U}_{M_r}$ are circulant matrices that are fully specified by their first rows given by vectors $[0, 1, \ldots, M_t - 1] - (M_t - 1)/2$ and $[0, 1, \ldots, M_r - 1] - (M_r - 1)/2$, respectively. Since a circulant matrix has full rank and the Bessel operation does not decrease its rank, from (52), we have $\text{rank}(\mathbf{B}_l) = M_t M_r$ for $N = 1$. It follows that, for all $N \geq 1$, we have $\text{rank}(\mathbf{B}_l) \geq M_t M_r$. Further considering the fact that $\sum_{l=0}^{L-1} \sum_{k=0}^{K-1} \text{rank}(\mathbf{R}_{l,k}^A) > LK$, we can rewrite (50) as

$$\Lambda \leq \min\{ M_r N, M_t M_r LK \}. \qquad (53)$$

In the case of the Laplacian AoA/AoD distribution, the matrix $\mathbf{B}_l$ has different values for its elements, but its rank property remains the same. Following a similar procedure, the same conclusion in (53) can be easily proved for the case of Laplacian-distributed AoAs/AoDs.

Equation (53) implies that once the ToA correlation is taken into account, the total degrees of freedom available in a UWB MIMO channel to be exploited for diversity gain is $M_t M_r LK$, regardless of the multipath amplitude correlation properties. This theoretical insight confirms our previous intuition in Section II that ToA correlation is a necessary complement to, rather than a reformulation of, the complex amplitude correlation.

It should be noted that the actual diversity gain achievable in a UWB MIMO channel depends on not only the rank properties of the multipath matrices but the exact conditions (particularly the eigenvalues) of these matrices as well. Therefore, although the degree of amplitude correlation has no impact on the maximum diversity order, it can have significant influence on the actual achievable diversity gain of the channel. Some quantitative results on the diversity gains achievable in realistic UWB MIMO systems will be presented in Section VI.

VI. NUMERICAL AND SIMULATION RESULTS

A. Numerical Results on the SF Covariance Matrix

In Section IV, we have shown that the SF covariance matrix $\mathbf{R}$ is given by the sum of L cluster SF covariance matrices $\mathbf{R}_l$. Each $\mathbf{R}_l$ can be decomposed as the Hadamard product of two matrices $\mathbf{A}_l$ and $\mathbf{B}_l$, where $\mathbf{A}_l$ is characterized by the multipath amplitude correlation, and $\mathbf{B}_l$ is characterized by the multipath ToA correlation. In what follows, we will show some numerical results to provide a direct visual understanding of the different impacts of $\mathbf{A}_l$ and $\mathbf{B}_l$ on $\mathbf{R}_l$.

We consider a scenario where a UWB access point transmits multimedia content to a digital display using MIMO technologies. The parameters of the UWB MIMO system are chosen to be $M_t = M_r = 2$, $d_p = 20$ cm, $d_q = 30$ cm, and $N = 256$. The system bandwidth is set to be $N\Delta f = 3 \times 528$ MHz according to the multiband (MB) OFDM UWB standard [22]. Based on the measured statistics for residential indoor environments [43],
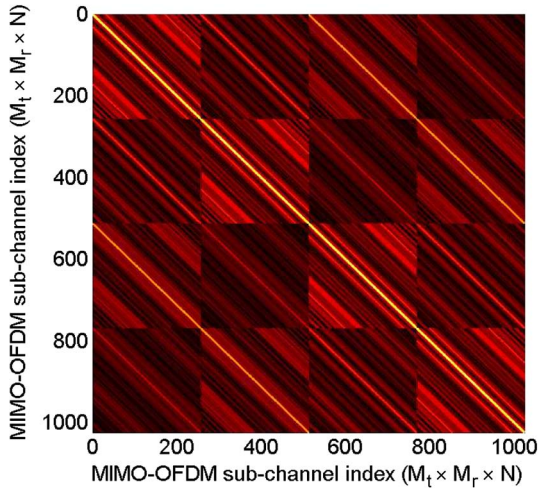
Fig. 4. Matrix $\mathbf{A}_l$ related to the multipath amplitude correlation ($M_t = M_r = 2$, $N = 256$, $N\Delta f = 3 \times 528$ MHz, $\tau_{\max} = 70$ ns, $L = 69$, and $\tau_{\mathrm{RMS}} = 11$ ns).
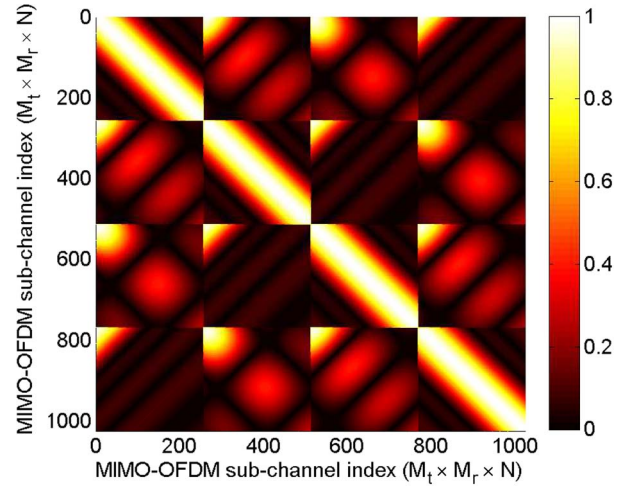

Fig. 5. Matrix $\mathbf{B}_l$ related to the multipath ToA correlation ($M_t = M_r = 2$, $N = 256$, $N\Delta f = 3 \times 528$ MHz, $d_p = 20$ cm, $d_q = 30$ cm, and the uniform AoA/AoD distribution from 0 to 2π).

we set the number of MPCs in the UWB channel $K = 69$, the delay spread $\tau_{\mathrm{RMS}} = 11$ ns, and the maximum reference ToA $\tau_{\max} = 70$ ns. To clearly illustrate the numerical results, the following simplifying assumptions are made.

1) The entire CIR is considered as one single cluster (i.e., $L = 1$), and the multipath ToA $\tau_{l,k}$ is uniformly distributed between 0 ns and $\tau_{\max}$.
2) An exponential power delay profile is adopted to calculate the multipath power using $\sigma_{l,k}^2 = \exp(-\tau_{l,k}/\tau_{\mathrm{RMS}})/\tau_{\mathrm{RMS}}$.
3) The AoAs and the AoDs are uniformly distributed from 0 to 2π.
4) The amplitude correlation of each tap is a random number depending on the number of irresolvable MPCs and their directional properties. A simple model is used to capture the essence of this phenomenon. We assume that the amplitude correlation coefficients are uniformly distributed within an interval $[\alpha_{\mathrm{low}}, 1]$, where $\alpha_{\mathrm{low}} \geq 0$ is a lower bound expressed as a cutoff linearly decreasing function of the antenna spacing x, i.e., $\alpha_{\mathrm{low}} = \max(0, 1 - x/0.3)$. Here, we assume that the lower bound reduces to zero at a spacing of 30 cm.

From (29) and (33), matrices $\mathbf{A}_l$ and $\mathbf{B}_l$ are computed, and the absolute values of their entries are shown in Figs. 4 and 5, respectively. The corresponding SF channel covariance matrix $\mathbf{R}_l$ is computed by (28) and shown in Fig. 6. The 4×4 distinguishable grids reflect the $M_t M_r \times M_t M_r$ spatial structure. For example, denote the two transmit antenna elements as T_1 and T_2, respectively, and the two received antenna elements as R_1 and R_2, respectively. The grid at the upper-left corner represents the autocovariance of the vector channel (consisting of 256 subcarriers) from T_1 to R_1. Inside each grid, the covariance values change due to varying subcarrier frequency spacing. From Figs. 4–6, it is observed that $\mathbf{B}_l$ has an important impact on decorrelating the MIMO channel.

The decorrelating effect of $\mathbf{B}_l$ on $\mathbf{R}_l$ depends on the system bandwidth. In Fig. 7, we compute the average absolute values of the elements in matrices $\mathbf{A}_l$, $\mathbf{B}_l$, and $\mathbf{R}_l$, respectively,
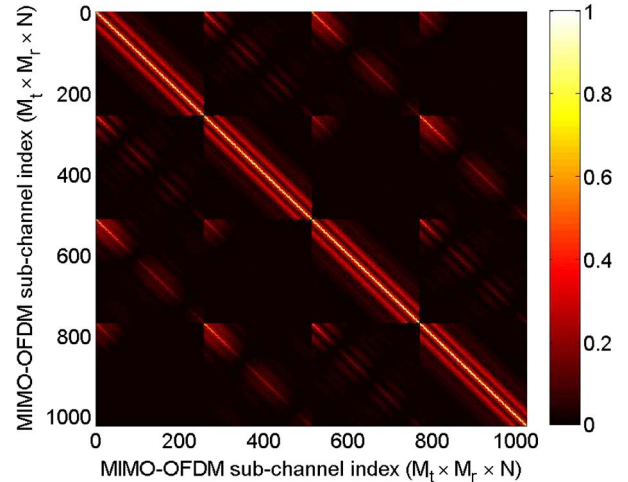

Fig. 6. SF covariance matrix $\mathbf{R} = \mathbf{A}_l \circ \mathbf{B}_l$ ($M_t = M_r = 2$, $N = 256$, $N\Delta f = 3 \times 528$ MHz, $\tau_{\max} = 70$ ns, $L = 69$, $\tau_{\mathrm{RMS}} = 11$ ns, $d_p = 20$ cm, $d_q = 30$ cm, and the uniform AoA/AoD distribution from 0 to 2π).

and show these average values as functions of the system bandwidth. It is observed that the decorrelating effect of $\mathbf{B}_l$ is significant (< 0.75) only if the system bandwidth exceeds 500 MHz, corresponding to the UWB system definition in the FCC [4]. Fig. 7 implies that the ToA correlation (i.e., matrix $\mathbf{B}_l$) can be neglected for conventional wideband MIMO systems with relatively small bandwidth but must be considered for UWB MIMO systems.

It is important to note that matrix $\mathbf{B}_l$ not only decorrelates the MIMO channel, but also introduces new "patterns" to the MIMO SF covariance matrix. Comparing Fig. 4 with Fig. 5, the different structures of matrices $\mathbf{A}_l$ and $\mathbf{B}_l$ are evident. It implies that the amplitude correlation and the ToA correlation differently contribute to the structure of the SF covariance matrix $\mathbf{R}_l$. Consequently, the decorrelating effect of $\mathbf{B}_l$ on $\mathbf{R}_l$ cannot be simply replaced by modifying $\mathbf{A}_l$ to have a lower degree of amplitude correlation. In other words, ToA correlation is not just a mathematical reformulation of the well-known complex amplitude correlation, but is a necessary complement to the
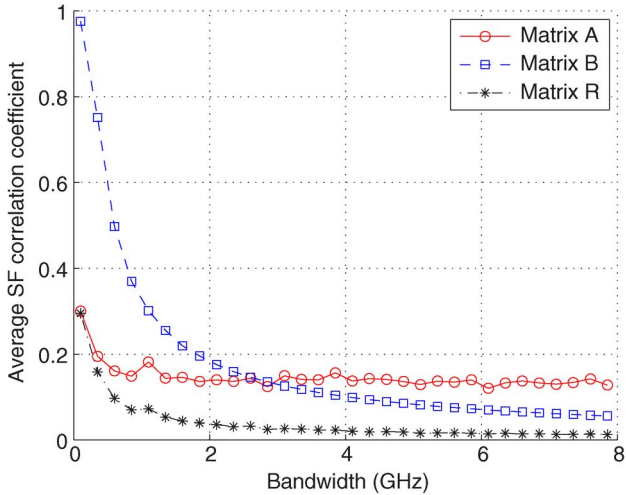
Fig. 7. Average absolute value of the SF correlation coefficients in matrices $\mathbf{A}_l$, $\mathbf{B}_l$, and $\mathbf{R}_l$ as functions of the system bandwidth ($M_t = M_r = 2$, $N = 256$, $N\Delta f = 3 \times 528$ MHz, $\tau_{\max} = 70$ ns, $L = 69$, $\tau_{\mathrm{RMS}} = 11$ ns, $d_p = 20$ cm, $d_q = 30$ cm, and the uniform AoA/AoD distribution from 0 to 2π).

amplitude correlation in the UWB regime. This observation corresponds to our theoretical analysis in Section V.

B. Numerical Results on the Spatial Correlation Function

Here, we aim to partly validate the proposed model by comparing the simulated channel properties with published measurement results. To our knowledge, no measurement result has been reported in the literature regarding the SF channel covariance matrix of UWB MIMO channels. However, the spatial correlation function of UWB MIMO channels has been measured in several campaigns [27]–[30].

The spatial correlation function describes the correlation, measured at a certain frequency, between two antenna elements as a function of antenna spacing. It can be easily calculated as $\rho^{p_1 q_1 n_1, p_2 q_2 n_2}$ in (12) by setting $n_1 = n_2$ and varying the antenna spacing values given by $d_{p_1} - d_{p_2}$ or $d_{q_1} - d_{q_2}$. Figs. 8 and 9 show the spatial correlation functions of the conventional UWB MIMO channel models and the proposed channel models at different frequency points, respectively. It is shown that the proposed model (with ToA correlation) can yield frequency-dependent spatial correlation, which is an intuitive channel property observed in several measurements [6], [27]–[30]. In contrast, conventional models (without ToA correlation) result in frequency-independent spatial correlation. Figs. 8 and 9 further prove that it is necessary to introduce ToA correlation into UWB channel modeling to better fit the measurement results.

C. Simulation Results of Alamouti-Coded MB-OFDM UWB Systems

Here, we aim to evaluate the impacts of ToA and amplitude correlations on the diversity performance of multiantenna UWB systems. Based on the MB-OFDM UWB system specified in the ECMA-368 standard [44], our simulation model extends the original single-input–single-output (SISO) system to a 2×1 multiple-input–single-output (MISO) system employing
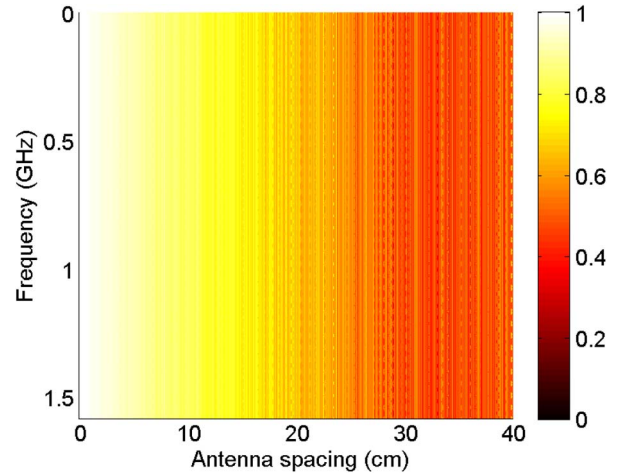

Fig. 8. Absolute value of the spatial correlation $\rho^{p_1 q_1 n_1, p_2 q_2 n_2}$ of two channel transfer functions as functions of the frequency and receive antenna spacing (without ToA correlation, $n_1 = n_2$, $N\Delta f = 3 \times 528$ MHz, $\tau_{\max} = 70$ ns, $L = 69$, $\tau_{\mathrm{RMS}} = 11$ ns, and the uniform AoA/AoD distribution from 0 to 2π).
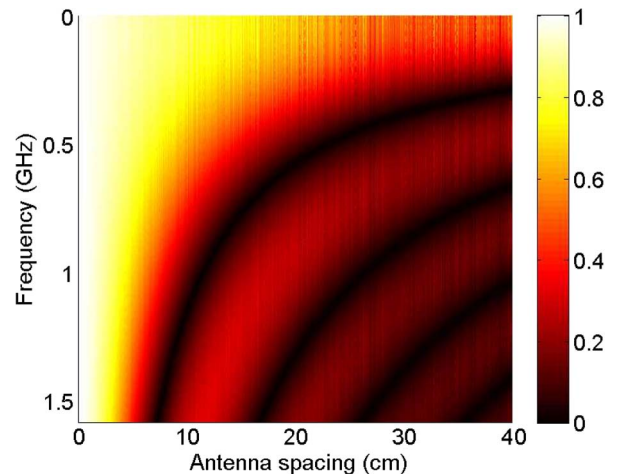

Fig. 9. Absolute value of the spatial correlation $\rho^{p_1 q_1 n_1, p_2 q_2 n_2}$ of two channel transfer functions as functions of the frequency and antenna spacing (with ToA correlation, $n_1 = n_2$, $N\Delta f = 3 \times 528$ MHz, $\tau_{\max} = 70$ ns, $L = 69$, $\tau_{\mathrm{RMS}} = 11$ ns, and the uniform AoA/AoD distribution from 0 to 2π).

Alamouti transmit diversity schemes. The physical layer functional blocks of our simulation model are shown in Fig. 10.

In the ECMA-368 standard, the overall 7.5-GHz bandwidth is divided into 14 subbands, where each subband has a bandwidth of 528 MHz. The center frequency of each OFDM symbol hops among different subbands according to predefined time–frequency codes (TFCs). In our simulation, we consider a popular TFC code that transmits OFDM symbols in the first band group, where the center frequencies of the three subbands are given by 3.432, 3.960, and 4.488 GHz. The TFC code that we use is $\{1, 2, 3, 1, 2, 3\}$. Correspondingly, the Alamouti space–time coding is performed over every two conjunctive OFDM symbols in the same subband.

The data are sent in packets, including the training preamble and the payload (information data). The time-domain OFDM signals are up-converted by a mixer to the desired frequency and pass through the channel by time-domain filtering with the CIR. The receiver first down-converts the received signals to
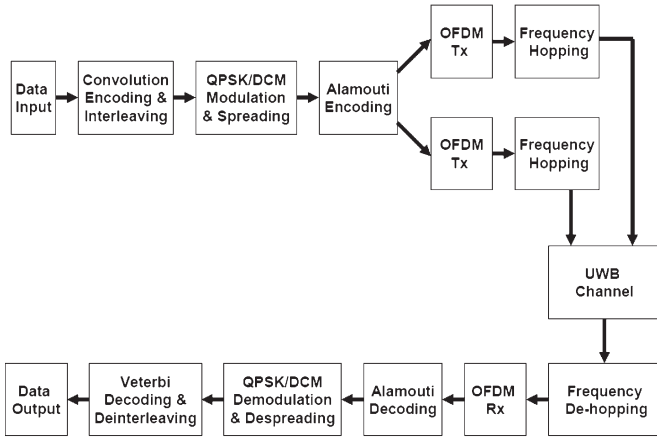
Fig. 10. Physical layer function blocks of an Alamouti-coded 2 × 1 MISO MB-OFDM UWB system.

Fig. 11. BER performance of an Alamouti-coded 2 × 1 MISO MB-OFDM UWB system with different channel correlation models and different values of transmit antenna spacing d_p (CM1, 480-Mb/s mode).

Fig. 12. BER performance of an Alamouti-coded 2 × 1 MISO MB-OFDM UWB system with different channel correlation models and different values of transmit antenna spacing d_p (CM3, 480-Mb/s mode).

the baseband. It then processes the frequency-domain preamble to estimate the channel, which is used to equalize the payload symbols. The payload symbols are then decoded and compared with the transmitted data to calculate the BER. In all simulations, the BER performance is calculated as the averaged BER of ten random channel realizations.

By applying different modulation, coding, and spreading techniques, the ECMA system can support eight data rates ranging from 53.3 to 480 Mb/s. In lower data-rate modes, the ECMA system spreads symbols over time and frequency to provide diversity gains in the time and frequency domains. To focus our results on the benefits of spatial diversity, we configure the system to the highest data-rate mode (i.e., 480 Mb/s), which uses dual-carrier modulation, a code rate of 3/4, and a spread factor of 1. In this case, the performance gains achieved by the 2 × 1 Alamouti system compared with the SISO system depend mainly on the exploitation of the spatial diversity.

To simulate the performance of the above system in realistic environments, we first generate UWB SISO CIRs using the standardized IEEE 802.15.3a UWB channel model [34], which was parameterized to represent four typical scenarios: CM1 for line of sight and a transmitter–receiver distance of 0–4 m, CM2 for nonline of sight (NLoS) and a distance of 0–4 m, CM3 for NLoS and a distance of 4–10 m, and CM4 for extreme NLoS multipath channels. The power of the baseband CIRs is normalized to 1, i.e., shadowing and path-loss effects are not considered. This is because we are only interested in the microdiversity performance determined by small-scale fading.

Based on the correlation model described in Sections III and IV, the above UWB SISO CIRs are used to generate three sets of UWB MISO CIRs: 1) MISO CIRs assuming amplitude correlation only, 2) MISO CIRs assuming ToA correlation only, and 3) MISO CIRs assuming both amplitude and ToA correlations. Laplacian distributions are adopted to describe AoA/AoD distributions in a cluster, and different values of transmit antenna spacing are used.

Different sets of MISO CIRs are then used to simulate the BER performance of the same Alamouti-coded MB-OFDM UWB system. The results of the Alamouti-coded MISO UWB system as well as the corresponding UWB SISO systems are shown in Figs. 11 and 12 for CM1 and CM3, respectively.
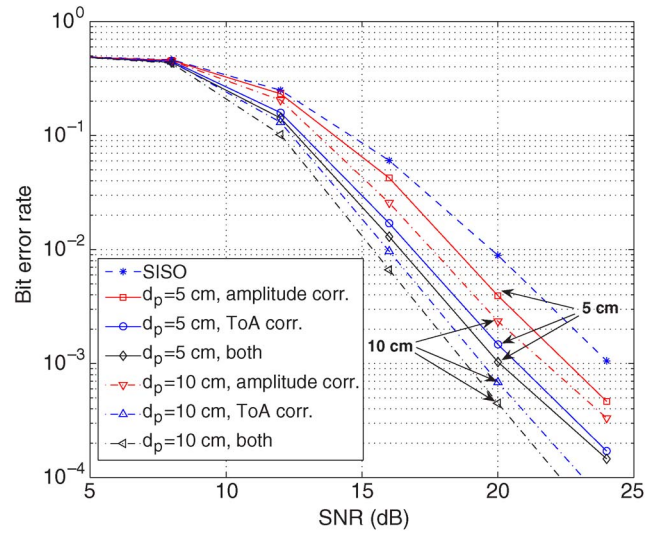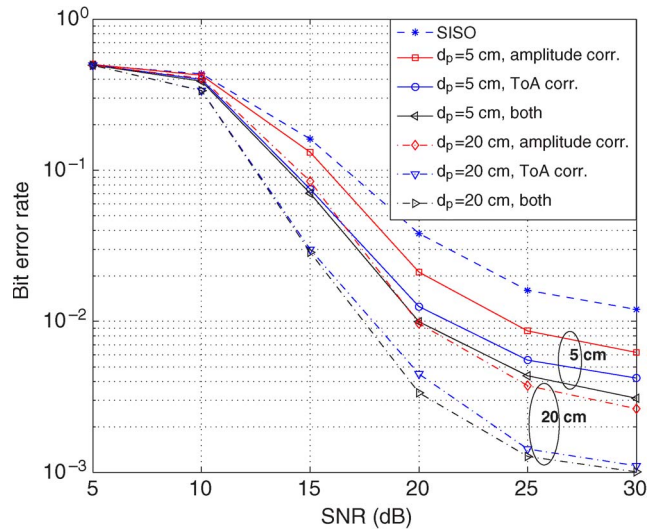
In both figures, it is observed that when both the ToA and amplitude correlations are taken into account, the diversity performance is better than the other two cases where either ToA or amplitude correlation is considered. This observation implies that neither the amplitude correlation nor the ToA correlation can solely capture the SF correlation property of UWB MIMO channels—a conclusion in agreement with the previous numerical results. Furthermore, ToA correlation appears to have a bigger impact on the BER performance than amplitude correlation, particularly when the antenna spacing is wider or the channel is more dispersive (CM3 represents more dispersive channels than CM1). These simulation results reinforce our previous conclusions that, in addition to complex amplitude correlation, ToA correlation is a necessary effect to consider in UWB MIMO channel modeling to facilitate accurate and realistic performance evaluation of UWB MIMO systems.

VII. Conclusion

This paper investigates the different roles of ToA and amplitude correlations in characterizing SF-correlated UWB MIMO channels. A UWB MIMO correlation model with improved accuracy has been proposed. Through physical intuition, theoretical analysis, numerical examples, and simulation results, we have concluded that multipath ToA correlation, which has been largely ignored so far in the literature, is a necessary and important complement to the well-known multipath amplitude correlation to fully characterize the SF correlation properties of UWB MIMO channels. We expect that this new insight into UWB MIMO channels will inspire further measurement campaigns and more realistic channel models to facilitate dependable design and performance evaluation of multigigabit UWB MIMO systems.

References

[1] A. J. Paulraj, R. Nabar, and D. Gore, *Introduction to Space-time Wireless Communications*. Cambridge, U.K.: Cambridge Univ. Press, 2003.

[2] C.-X. Wang, D. Yuan, H.-H. Chen, and W. Xu, "An improved deterministic SoS channel simulator for efficient simulation of multiple uncorrelated Rayleigh fading channels," *IEEE Trans. Wireless Commun.*, vol. 7, no. 9, pp. 3307–3311, Sep. 2008.

[3] C.-X. Wang, M. Pätzold, and D. Yuan, "Accurate and efficient simulation of multiple uncorrelated Rayleigh fading waveforms," *IEEE Trans. Wireless Commun.*, vol. 6, no. 3, pp. 833–839, Mar. 2007.

[4] B. Allen, M. Dohler, E. E. Okon, W. Q. Malik, A. K. Brown, and D. J. Edwards, *Ultra-Wideband Antennas and Propagation for Communications, Radar and Imaging*. Chichester, U.K.: Wiley, 2007.

[5] W. Q. Malik and D. J. Edwards, "Measured MIMO capacity and diversity gain with spatial and polar arrays in ultrawideband channels," *IEEE Trans. Commun.*, vol. 55, no. 12, pp. 2361–2370, Dec. 2007.

[6] W. Q. Malik, "Spatial correlation in ultrawideband channels," *IEEE Trans. Wireless Commun.*, vol. 7, no. 2, pp. 604–610, Feb. 2008.

[7] T. Kaiser, F. Zheng, and E. Dimitrov, "An overview of ultra-wideband systems with MIMO," *Proc. IEEE*, vol. 97, no. 2, pp. 285–312, Feb. 2009.

[8] C.-X. Wang, M. Pätzold, and Q. Yao, "Stochastic modeling and simulation of frequency correlated wideband fading channels," *IEEE Trans. Veh. Technol.*, vol. 56, no. 3, pp. 1050–1063, May 2007.

[9] X. Cheng, C.-X. Wang, D. I. Laurenson, S. Salous, and A. V. Vasilakos, "An adaptive geometry-based stochastic model for non-isotropic MIMO mobile-to-mobile channels," *IEEE Trans. Wireless Commun.*, vol. 8, no. 9, pp. 4824–4835, Sep. 2009.

[10] J. P. Kermoal, L. Schumacher, K. I. Pedersen, and P. E. Mogensen, "A stochastic MIMO radio channel model with experimental validation," *IEEE J. Sel. Areas Commun.*, vol. 20, no. 6, pp. 1211–1226, Aug. 2002.

[11] C.-X. Wang, X. Hong, H. Wu, and W. Xu, "Spatial temporal correlation properties of the 3GPP spatial channel model and the Kronecker MIMO channel model," *EURASIP J. Wireless Commun. Netw.*, vol. 2007, pp. 1–9, 2007, Article ID 39871, DOI:10.1155/2007/39871.

[12] W. Weichselberger, M. Herdin, H. Ozcelik, and E. Bonek, "A stochastic MIMO channel model with joint correlation of both link ends," *IEEE Trans. Wireless Commun.*, vol. 5, no. 1, pp. 90–100, Jan. 2006.

[13] A. M. Sayeed, "Deconstructing multiantenna fading channels," *IEEE Trans. Signal Process.*, vol. 50, no. 10, pp. 2563–2579, Oct. 2002.

[14] A. Abdi and M. Kaveh, "A space-time correlation model for multielement antenna systems in mobile fading channels," *IEEE J. Sel. Areas Commun.*, vol. 20, no. 3, pp. 550–560, Mar. 2002.

[15] A. Abdi, J. A. Barger, and M. Kaveh, "A parametric model for the distribution of the angle of arrival and the associated correlation function and power spectrum at the mobile station," *IEEE Trans. Veh. Technol.*, vol. 51, no. 3, pp. 425–434, Mar. 2002.

[16] S. Gazor and H. S. Rad, "Space-time-frequency characterization of MIMO wireless channels," *IEEE Trans. Wireless Commun.*, vol. 5, no. 9, pp. 2369–2375, Sep. 2006.

[17] L. Schumacher and B. Raghothaman, "Closed-form expressions for the correlation coefficient of directive antennas impinged by a multimodal truncated Laplacian PAS," *IEEE Trans. Wireless Commun.*, vol. 4, no. 4, pp. 1351–1359, Jul. 2005.

[18] P. D. Teal, T. D. Abhayapala, and R. A. Kennedy, "Spatial correlation in non-isotropic scattering scenarios," in *Proc. IEEE ICASSP*, Orlando, FL, May 2002, pp. 2833–2836.

[19] L. Schumacher, K. I. Pedersen, and P. E. Mogensen, "From antenna spacings to theoretical capacities—Guidelines for simulating MIMO systems," in *Proc. IEEE Int. Symp. PIMRC*, Lisbon, Portugal, Sep. 2002, pp. 587–592.

[20] W. Su, Z. Safar, and K. Liu, "Towards maximum achievable diversity in space, time and frequency: Performance analysis and code design," *IEEE Trans. Wireless Commun.*, vol. 4, no. 4, pp. 1847–1857, Jul. 2005.

[21] A. Sadek, W. Su, and K. Liu, "Diversity analysis for frequency-selective MIMO-OFDM systems with general spatial and temporal correlation model," *IEEE Trans. Commun.*, vol. 54, no. 5, pp. 878–888, May 2006.

[22] W. P. Siriwongpairat, W. Su, M. Olfat, and K. J. R. Liu, "Multiband-OFDM MIMO coding framework for UWB communication systems," *IEEE Trans. Signal Process.*, vol. 54, no. 1, pp. 214–224, Jan. 2006.

[23] L. Q. Yang and G. B. Giannakis, "Space-time coding for impulse radio," in *Proc. IEEE Conf. Ultra Wideband Syst. Technol.*, Baltimore, MD, May 2002, pp. 235–239.

[24] L. Zhiwei, B. Premkumar, and A. S. Madhukumar, "MMSE detection for high data rate UWB MIMO systems," in *Proc. IEEE VTC*, Los Angeles, CA, Sep. 2004, pp. 1463–1467.

[25] J. Adeane, W. Q. Malik, I. J. Wassell, and D. J. Edwards, "A simple correlated channel model for ultrawideband MIMO systems," *IET Microw., Antennas Propag.*, vol. 1, no. 6, pp. 1177–1181, Dec. 2007.

[26] X. Hong, C.-X. Wang, B. Allen, and W. Q. Malik, "A correlation-based double-directional stochastic channel model for multiple-antenna UWB systems," *IET Microw., Antennas Propag.*, vol. 1, no. 6, pp. 1182–1191, Dec. 2007.

[27] J. Liu, B. Allen, W. Q. Malik, and D. J. Edwards, "On the spatial correlation of MB-OFDM ultra wideband transmissions," in *Proc. COST 273 Meeting*, Bologna, Italy, Jan. 2005.

[28] H. Agus, J. Nielsen, and R. J. Davies, "Temporal and spatial correlation analysis for indoor UWB channel," in *Proc. Wireless*, Calgary, AB, Canada, Jul. 2005, pp. 102–110.

[29] C. Prettie, D. Cheung, L. Rusch, and M. Ho, "Spatial correlation of UWB signals in a home environment," in *Proc. IEEE Conf. Ultra Wideband Syst. Technol.*, Baltimore, MD, May 2002, pp. 65–69.

[30] J. Liu, B. Allen, W. Q. Malik, and D. J. Edwards, "A measurement based spatial correlation analysis for MB-OFDM ultra wideband transmissions," in *Proc. LAPC*, Loughborough, U.K., Apr. 2005.

[31] X. Hong, C.-X. Wang, J. S. Thompson, B. Allen, and W. Q. Malik, "Deconstructing space–frequency correlated ultrawideband MIMO channels," in *Proc. ICUWB*, Hanover, Germany, Sep. 2008, pp. 47–50, invited paper.

[32] A. A. M. Saleh and R. A. Valenzuela, "A statistical model for indoor multipath propagation," *IEEE J. Sel. Areas Commun.*, vol. SAC-5, no. 2, pp. 128–137, Feb. 1987.

[33] W.-J. Chang and J.-H. Tarng, "Effects of bandwidth on observable multipath clustering in outdoor/indoor environments for broadband and ultrawideband wireless systems," *IEEE Trans. Veh. Technol.*, vol. 56, no. 4, pp. 1913–1923, Apr. 2002.

[34] J. Foerster *et al.*, "Channel modeling sub-committee report final," IEEE P802.15-02/368r5-SG3a, 2002. [Online]. Available: http://www.ieee802.org/15/pub/2002/Nov02/

[35] R. J. M. Cramer, R. A. Scholtz, and M. Z. Win, "Evaluation of an ultrawide-band propagation channel," *IEEE Trans. Antennas Propag.*, vol. 50, no. 5, pp. 561–570, May 2002.

[36] K. Haneda, J. Takada, and T. Kobayashi, "Double directional ultra wideband channel characterization in a line-of-sight home environment," *IEICE Trans. Fundam.*, vol. E88-A, no. 9, pp. 2264–2271, Sep. 2005.

[37] Spatial Channel Model for Multiple Input Multiple Output (MIMO) Simulations (Rel. 6), 3GPP, TR 25.996, 2003.

[38] D. Cassioli, M. Z. Win, and A. F. Molisch, "The ultra-wide bandwidth indoor channel: From statistical model to simulations," *IEEE J. Sel. Areas Commun.*, vol. 20, no. 6, pp. 1247–1257, Aug. 2002.

[39] V. Erceg *et al.*, "TGn Channel Models," IEEE Std. 802.11 document 03/940r4, 2004.

[40] T. A. Lamahewa, R. A. Kennedy, T. D. Abhayapala, and T. Betlehem, "MIMO channel correlation in general scattering environments," in *Proc. 7th Australian Commun. Theory Workshop*, Perth, Australia, Feb. 2006, pp. 93–98.

[41] A. F. Molisch, "Ultrawideband propagation channels-theory, measurement, and modeling," *IEEE Trans. Veh. Technol.*, vol. 54, no. 5, pp. 1528–1545, Sep. 2005.

[42] R. A. Horn and C. R. Johnson, *Matrix Analysis*. Cambridge, U.K.: Cambridge Univ. Press, 1985.

[43] S. S. Ghassemzadeh, R. Jana, C. W. Rice, W. Turin, and V. Tarokh, "Measurement and modeling of an ultra-wide bandwidth indoor channel," *IEEE Trans. Commun.*, vol. 52, no. 10, pp. 1786–1796, Oct. 2004.

[44] High Rate Ultra Wideband PHY and MAC Std., ECMA-368, Dec. 2007.

Xuemin Hong received the B.Sc. degree in communication engineering from Beijing Information Science and Technology University, Beijing, China, in 2004 and the Ph.D. degree in wireless communications from Heriot-Watt University, Edinburgh, U.K., in 2008.

From 2004 to 2005, he was with the Centre for Telecommunication Research, King's College London, London, U.K. From January 2009 to July 2009, he was a Postdoctoral Research Fellow with the Department of Electrical and Computer Engineering, University of Waterloo, Waterloo, ON, Canada. Since August 2009, he has been a Postdoctoral Research Associate with the Joint Research Institute for Signal and Image Processing, Heriot-Watt University, where he is also the Network Manager of the "U.K.–China Science Bridges: R&D on (B)4G Wireless Mobile Communications". He has published 20 technical papers in major international journals and conferences, as well as one book chapter in the area of wireless communications. His research interests include multiple-input–multiple-output and cooperative systems, ultrawideband systems, wireless radio channel modeling, cognitive radio networks, and (beyond) fourth generation [(B)4G] wireless communications.

Dr. Hong was a Publicity Chair for the IEEE 2010 International Conference on Communications and Mobile Computing and a technical program committee member for several international conferences.

Cheng-Xiang Wang (S'01–M'05–SM'08) received the B.Sc. and M.Eng. degrees in communication and information systems from Shandong University, Jinan, China, in 1997 and 2000, respectively, and the Ph.D. degree in wireless communications from Aalborg University, Aalborg, Denmark, in 2004.

From 2000 to 2001, he was a Research Assistant with the Technical University of Hamburg-Harburg, Hamburg, Germany. From 2001 to 2005, he was a Research Fellow with the University of Agder, Grimstad, Norway. In 2004, he was a Visiting Researcher with Siemens AG-Mobile Phones, Munich, Germany. Since 2005, he has been with Heriot-Watt University, Edinburgh, U.K., first as a Lecturer and then as a Reader in 2009. He is also an Honorary Fellow with the University of Edinburgh, Edinburgh, U.K., a Chair Professor with Shandong University, a Guest Professor with Huazhong University of Science and Technology, Wuhan, China, an Adjunct Professor with Guilin University of Electronic Technology, Guilin, China, and a Guest Researcher with Xidian University, Xi'an, China. He is leading several projects funded by the U.K. Engineering and Physical Sciences Research Council (EPSRC), Mobile VCE, and industries including the Research Councils U.K.-funded "U.K.–China Science Bridges: R&D on (B)4G Wireless Mobile Communications." He is currently serving as an Editor for *Wireless Communications and Mobile Computing Journal* (Wiley), *Security and Communication Networks Journal* (Wiley), and the *Journal of Computer Systems, Networks, and Communications* (Hindawi). He has published one book chapter and over 130 papers in refereed journals and conference proceedings. His current research interests include wireless channel modeling and simulation, cognitive radio networks, vehicular communication networks, green radio communications, cooperative (relay) communications, cross-layer design of wireless networks, multiple-input–multiple-output, orthogonal frequency division multiplexing, ultrawideband, and (B)4G wireless communications.

Dr. Wang is a member of the Institution of Engineering and Technology, a Fellow of the Higher Education Academy, and a Member of the EPSRC Peer Review College. He was an Editor for the IEEE TRANSACTIONS ON WIRELESS COMMUNICATIONS from 2007 to 2009. He is the leading Guest Editor for the IEEE JOURNAL ON SELECTED AREAS IN COMMUNICATIONS, Special Issue on Vehicular Communications and Networks. He served or is serving as a technical program committee (TPC) member, the TPC Chair, and the General Chair for about 60 international conferences. He was the recipient of the IEEE Global Telecommunications Conference 2010 Best Paper Award. He is listed in the "Dictionary of International Biography 2008 and 2009," "Who's Who in the World 2008 and 2009," "Great Minds of the 21st Century 2009," and "2009 Man of the Year."

John Thompson (M'03) received the B.Eng. and Ph.D. degrees from the University of Edinburgh, Edinburgh, U.K., in 1992 and 1996, respectively.

From July 1995 to August 1999, he was a Postdoctoral Researcher with the University of Edinburgh, funded by the U.K. Engineering and Physical Sciences Research Council and Nortel Networks. In September 1999, he became a Lecturer with the School of Engineering and Electronics, University of Edinburgh, where in October 2005, he was promoted to the position of Reader. He has published approximately 160 papers to date, including a number of invited papers, book chapters, and tutorial talks, as well as coauthoring an undergraduate textbook on digital signal processing. His research interests currently include signal processing algorithms for wireless systems, antenna array techniques, and multihop wireless communications.

Dr. Thompson is the founding Editor-in-Chief of the *IET Signal Processing Journal*. He is a Technical Program Cochair for the 2010 IEEE Global Telecommunications Conference to be held in Miami, FL, and also has served in the same role for the IEEE International Conference on Communications, which was held in Glasgow, U.K., in June 2007.

Ben Allen (SM'05) received the Ph.D. degree from the University of Bristol, Bristol, U.K., in 2001.

In 2002, he joined Tait Electronics Ltd., Christchurch, New Zealand, before becoming a Research Fellow with the Centre for Telecommunications Research, King's College London, London, U.K. In 2003, he became a member of the academic staff. Between 2005 and 2010, he was with the Department of Engineering Science, University of Oxford, Oxford, U.K. He is currently a Professor of computer science with the Department of Computer Science and Technology, University of Bedfordshire, Luton, U.K. He has widely published in the area of wireless systems and has an established track record of wireless technology innovation that has been built up through collaboration between industry and academia. His research interests include wideband wireless systems, antennas, propagation, and waveform design.

Prof. Allen is a Fellow of the Institution of Engineering and Technology and a Member of the editorial board of the *IET Microwaves, Antennas, and Propagation Journal*. He has received several awards.

Wasim Q. Malik (S'97–M'00–SM'08) received the Ph.D. degree in electrical engineering from the University of Oxford, Oxford, U.K., in 2005.

From 2005 to 2007, he was a Research Fellow with the University of Oxford. From 2005 to 2007, he was a Research Fellow with the Massachusetts Institute of Technology, Cambridge, and Harvard Medical School, Boston, MA. He is currently an Instructor with Harvard Medical School and is affiliated with the Massachusetts General Hospital. He holds visiting academic appointments with the Massachusetts Institute of Technology and Brown University, Providence, RI. He is also with the U.S. Department of Veterans Affairs. He serves as an International Expert Evaluator for the Research Council of Norway. He is an Editor of the *International Journal of Ultra Wideband Communications & Systems*. He served as a Guest Editor for the *IET Microwaves Antennas & Propagation* Special Issue on "Antennas systems and propagation for future wireless communications" and the *International Journal of Digital Multimedia Broadcasting* Special Issue on "Broadcast communications and broadcasting in confined areas."

Dr. Malik is the Chair of the IEEE Engineering in Medicine and Biology Society Boston Section, a Member of the Society for Neuroscience, and a Member of the IEEE Communications Society. He served as the Technical Program Committee Chair at the Institution of Engineering and Technology (IET) Workshop on Smart Antennas (London, U.K., 2007) and the IET Ultrawideband Symposium (Grenoble, France, 2007), the General Chair at the IET Workshop on Wideband and Ultrawideband Systems & Technologies (London, 2008), and a General Cochair at the IEEE International Conference on Ultrawideband (Hannover, Germany, 2008). He was a recipient of the Association for Computing Machinery Recognition of Service Award (2000), the Best Paper Award at the Automated Radio Frequency (RF) and Microwave Measurement Society RF and Microwave Conference (2006), the English-Speaking Union Lindemann Fellowship (2007), and the Center for Integration of Medicine and Innovative Technology Career Development Award (2010).

Xiaohu Ge (M'09) received the Ph.D. degree in communication and information engineering from Huazhong University of Science and Technology (HUST), Wuhan, China, in 2003.

From January 2004 to December 2005, he was an Assistant Researcher with Ajou University, Seoul, Korea, and the Politecnico Di Torino, Turin, Italy. Since December 2005, he has been with HUST, where he is currently an Associate Professor with the Department of Electronics and Information Engineering. He is a Project Review Expert for the Chinese Ministry of Science and Technology and the National Natural Science Foundation of China. He is the Editor for the international journal *KSII Transactions on Internet and Information Systems*. His research interests include the areas of mobile communication, traffic modeling in wireless networks, as well as interference modeling in wireless communications.

Dr. Ge has been actively involved since 2005 in the organization of more than ten international conferences, such as the Publicity Chair of IEEE Europecomm 2011 and a Cochair of the workshop on Green Communication of Cellular Networks at the 2010 IEEE International Conference on Green Computing and Communications.